


Vibro-Impact Capsule Under Different Conditions of Friction



Ngoc-Tuan La, Thanh-Toan Nguyen, Ky-Thanh Ho, Quoc-Huy Ngo,
and Van-Du Nguyen 

1 Introduction

Recently, the application of vibration-driven locomotion in capsule robots has been widely considered. A capsule robot is a platform that can self-propel in a resistive environment but can be encapsulated in a smooth form, without any external propellers [1]. The design of the locomotion systems is based on the two major mechanics of the interaction between the internal mass and the system body, known as vibration-driven and vibro-impact-driven principles.

In vibration-driven locomotion systems, initially proposed by Chernous'ko [2], the rectilinear motion can be achieved by using an additional internal mass interacting with the body frame. On the one hand, the simplicity in structure of the system makes it well suitable to form capsule robots. On the other hand, it is required that the relative motion of the internal mass must be controlled to have an exact form of multiphase accelerations. The vibration-driven platforms have been extensively investigated from various aspects, such as designing, modeling, and experimental validation [3–10]; dynamical analysis [11–16]; and optimal progression and motion control [14, 17–24]. The internal mass can connect with the body by means of an elastic spring to enhance the resonant characteristics. Various methods have been proposed to actuate the internal drives, including DC-motor-driven pendulum [25], unbalance rotor [10, 26], electromagnetic mechanisms [14, 27–29], and solenoid [15], [28]. Several useful guidelines for the design and control of bistable vibration-driven locomotion systems were also provided. However, for periodic relative

N.-T. La
Vinh University of Technology Education, Vinh, Vietnam

T.-T. Nguyen · K.-T. Ho · Q.-H. Ngo · V.-D. Nguyen (✉)
Thai Nguyen University of Technology, Thai Nguyen University, Thai Nguyen, Vietnam
e-mail: vandu@tnut.edu.vn

motion of the internal mass, the friction must be anisotropic, i.e., friction force in the forward direction is smaller than that in backward trend (e.g., [7, 15, 18, 30, 31]). As a whole, the major concerns of the first design option would be the complex motion control and special demand of anisotropic friction.

In a vibro-impact-driven locomotion system, the internal mass oscillates and has periodical impacts with the system body [32], resulted in a jump-up of the inertial force. When the impact force exceeds the friction force, the system is displaced. The drifting oscillator proposed by Pavlovskaja et al. [33] provided a fundamental model for distinctive locomotion systems. The internal mass (impact oscillator) has been driven by various ways, for example, a system of motor and cam mechanism [34], solenoid working with sinusoidal in an RLC circuit [35, 36], electromagnetic device [37, 38], linear motor [9], and electrodynamic shaker [16, 22]. The system can be either position feedback controlled [23] or reverse the impact side [5] to obtain the expected direction of motion.

In previous experimental studies on the locomotion platforms, the friction force was considered as either an isotropic [13] or an anisotropic [18] resistance. Several experimental studies have been investigated. However, the effect of various friction levels on the system behavior was not fully examined.

With isotropic assumption, the excitation force was usually compared with the friction force magnitude, using the force ratio between the excited amplitude and the friction force. The motion of the system was examined for different levels of the excitation by varying such force ratio (see, e.g., in [5, 9, 25, 32, 33]). In experimental studies, a preset and unchanged dry friction was usually implemented (see [8, 9, 22, 39, 40]). The dependence of the system response as a function of the friction variable has rarely been experimentally examined [35, 41]. Several interesting phenomena have been observed [9, 23]. For example, when the elastic force acting on the system body becomes greater than the friction threshold, the system may move backward [23]. In some situations, applying a larger excited amplitude would not improve the performance of the system [9]. It is regretted that such interesting interpretations were carried out at a certain value of friction. Besides, the magnitude of excitation force was counted by comparing it with the friction. The results of our study revealed that with the same force ratio, different values of friction provided different average velocities and also the direction of the progression. Recently, several interesting investigations were implemented, focusing on the efficacy of the model and its feasibility under various isotropic frictional conditions [42, 43]. Various capsule-intestine contact conditions for which the capsule moves include four cases of isotropic friction: flat-open synthetic small intestine in a flat form and in a curve form, collapsed and loose synthetic small intestine, and contractive synthetic intestine whose inner diameter was smaller than the capsule's external diameter.

Several studies were made for anisotropic friction, where the friction force in forward motion is different from that in backward motion. However, most of the experimental studies assumed that the forward friction is smaller than the backward friction [18, 30]. Such systems either were built with asymmetric legs [30] or were able to move downward on an inclined chute only [18]. In our study, the response

of the locomotion system was experimentally examined under a more general case of anisotropic friction, where the resistant force in the forward direction is larger than that in the backward motion. The experimental setup was built similar to the one implemented in [18], but the forward direction was considered to be the upward trend on an inclined chute. Moreover, the resistant force consisted of two contents: one preset and an adjustable level.

This report presents an experimental study on the vibro-impact-driven capsule, working under different friction conditions, including isotropic and anisotropic resistant forces. The experimental setup made it possible to vary the friction force easily.

2 Experimental Setup

The model of a vibro-impact locomotion system is shown in Fig. 1a.

An internal mass m_1 is connected with the system frame mass m_2 by a spring with stiffness k and a linear viscous damper c . A harmonic sinusoidal force F_m acts on both masses as an interaction force. The impact stiffness is modeled as a linear spring k_0 . X_1 and X_2 are the absolute displacements of the two masses m_1 and m_2 , respectively. At the initial stage, the two masses gave a gap G . Whenever $X_1 - X_2$ overcomes the gap G , impact happens, and thus, the system can move forward. A dry friction force F_S presents the environment resistance acting against the motion of the system frame.

In this study, the experimental apparatus was made to provide either isotropic friction or anisotropic friction resistance. When the system is arranged horizontally, as shown in Fig. 1a, the resistant forces in forward and backward motions are considered to be the same, i.e., the friction force is isotropic. The setup was then developed to examine the anisotropic friction, referring to previous studies [7, 18],

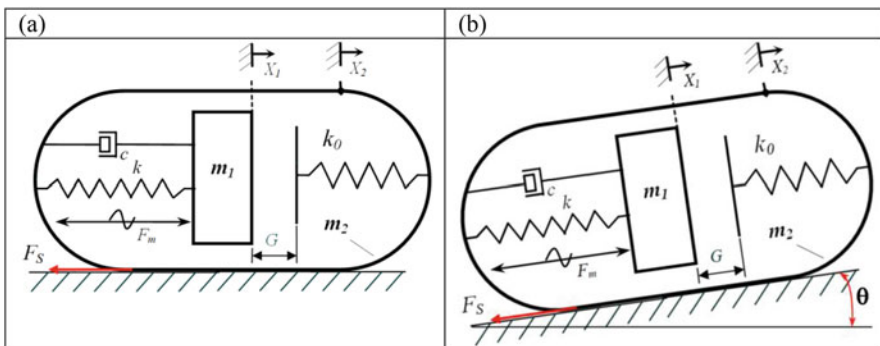


Fig. 1 Models of the vibro-impact locomotion system with (a) isotropic friction and (b) anisotropic friction

where the forward resistance is smaller than the backward resistance. When the prototype is placed on an inclined surface, as shown in Fig. 1b, the anisotropy characteristic of the friction coefficients can be achieved by making use of the gravity effect.

When the prototype is moving on the chute, the equivalent friction force consists of two parts: one is the dry friction force F_S , and the other is the gravitational force component along the inclined chute direction. In contrast to [7, 18], this study assigned the upward direction as the forward motion, i.e., the forward resistance force is larger than the backward resistance. Increasing the inclined angle, θ leads to increase in the ratio between forward friction and backward friction. In this study, such ratio will be called the anisotropic ratio. Two levels of the ratio were examined, represented by two values of the inclined angle, θ .

The detailed experimental setup is described in Fig. 2, where the experimental schema is depicted in Fig. 2a and a photograph of the realized apparatus is shown in Fig. 2b.

In Fig. 2, a mini electrodynamic shaker (1) was used to provide relative oscillations between the two masses. The shaker was fixed on a rolling slider guide (4), provided that a tiny rolling friction force is available when the system moves. The slider can be adjusted to provide a certain inclined angle θ , with respect to the horizontal surface. An additional mass (2) was fixed on the shaker shaft. Exciting the shaker by a sinusoidal current, a linear oscillation of the shaker shaft with respect to the shaker body was generated. The internal mass m_1 involves the addition of mass and the shaker shaft weight. A noncontact position sensor (7) was used to measure the relative motion of the internal mass m_1 . The displacement of the shaker body was collected by a linear variable displacement transformer (LVDT). The body shaker, including the sensors and the carbon tube, is denoted as the mass m_2 . An obstacle block (3) was used to absorb the impact force. A carbon tube (5), which has a tiny weight, is connected with the shaker body by means of a flexible joint and can be slid inside a coupled V-block. This mechanism provided the ability to adjust the resistance (friction) force when the system is moving. The detailed mechanism of providing preset friction is depicted in Fig. 3.

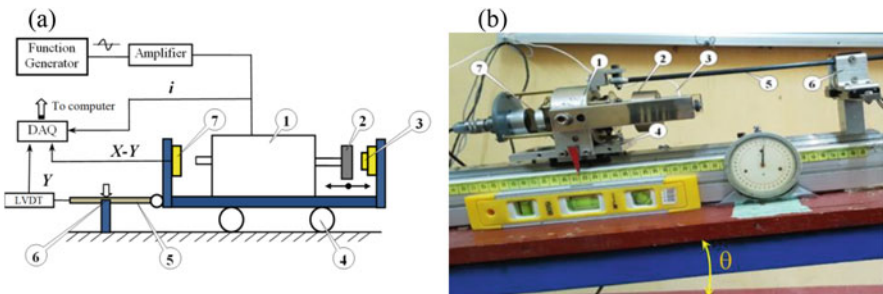


Fig. 2 Models of the vibro-impact locomotion system with (a) isotropic friction and (b) anisotropic friction

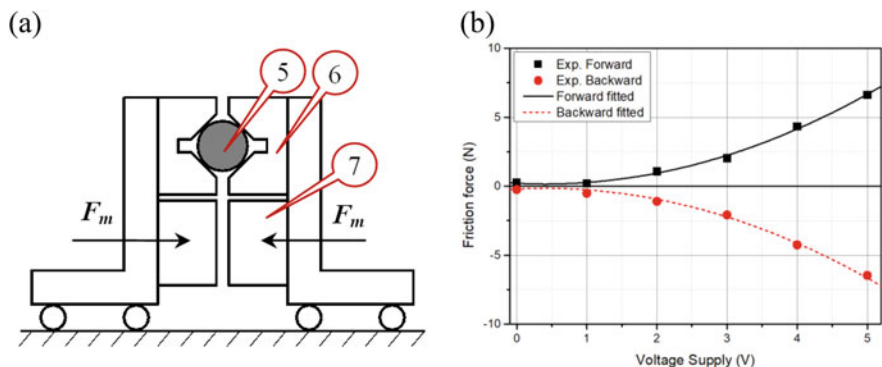


Fig. 3 Varying the friction force: (a) apparatus structure and (b) the dependency of friction force on the supplied voltage

Table 1 Experimental factors

Factor	Notation	Value	Unit
Internal mass	m_1	0.518	Kg
Body mass	m_2	1.818	Kg
Impact gap	G	0.5	mm
Friction force	F_S	2.4; 6.8; and 13.6	N
Force ratio	$\alpha = A/F_S$	0.59; 0.79; 0.99; and 1.19	–
Inclined angle	θ	0; 2.5 and 5	$^\circ$
Excitation frequency	f_{exc}	15	Hz

As depicted in Fig. 3a, the carbon tube (5) connects with and moves together with the system body. The tube is clamped by means of two aluminum V-block (6), which are fixed on two electromagnets (7). By adjusting the electrical current supplied to the electromagnets, it is able to obtain the expected force clamping the carbon tube. As a result, the sliding friction force exerting on the tube when moving can be predetermined. Moving the body at a slow and steady speed, the preset friction force corresponding to the voltage supplied can be collected (see more details in [41]). Figure 3b presents the relationship between the control voltage and the slide friction force. Based on such relationship, the preset friction between the system and the environment can be adjusted, without changing the weight of the system. Table 1 shows the values of experimental parameters.

3 Results and Discussions

Figure 4 shows the time history of the motion X_1 of the internal mass and the motion X_2 of the whole body for various preset friction levels and inclined angles.

Overall, the system works under higher preset friction force would have more ability to move forward. Besides, increasing the inclined angle θ resulted in either

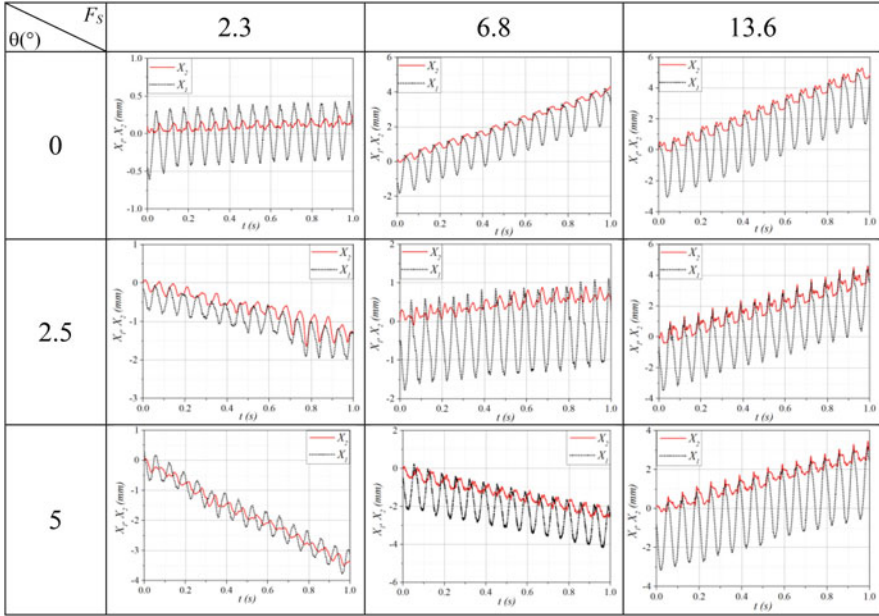


Fig. 4 Time history of the motions of the two masses for various values of preset friction and inclined angle; a force ratio $\alpha = 0.59$ and an excitation frequency of 15 Hz were applied

backward motion or a lower forward progression rate. It is reasonable due to the effect of the gravity force, which always tends to draw the system to move backward.

As shown in the first-row subplots of Fig. 4, under the isotropic friction ($\theta = 0^\circ$), increasing the preset friction would provide a higher progression rate. For anisotropic friction ($\theta = 2.5^\circ$ and $\theta = 5^\circ$), a low preset friction resulted in a backward motion, whereas the highest preset friction provided the fastest forward motion.

In order to examine the moving direction as well as the progression rate of the system under the concurrent effect of the force ratio and the preset friction, three sets for inclined angles of 0° , 2.5° , and 5° were implemented. Each set includes 12 runs, combining three levels of friction ($F_S = 2.3$ N, 6.8 N, and 13.6 N), and four levels of the force ratio ($\alpha = 0.59, 0.79, 0.99, \text{ and } 1.19$) were implemented. The progression velocity obtained is represented by two-parameter contour plots in Fig. 5. The plots were made directly from experimental data by OriginLab[®] software. In Fig. 5, the areas of backward motion (denoted by the sign “-”) were represented by gray, dark grey, violet, blue, purple, and navy, whereas the areas of forward motion (denoted by the sign “+”) were shown in green, yellow, orange, and magenta.

As can be seen, in the investigated ranges of the two parameters, for isotropic friction (Fig. 5a), the system had forward motion for most combination values of the preset friction force and the force ratio. The system moved backward in a small range of the force ratio $\alpha \in [1.05, 1.19]$ combined with a large range of friction force

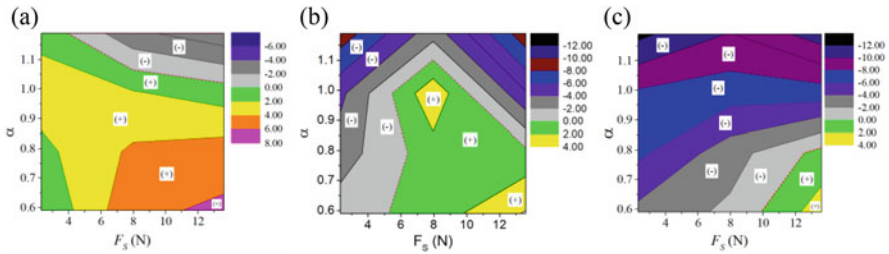


Fig. 5 (Color online) Contour plots of the progression rate with respects to the preset friction force F_s and the force ratio α for (a) $\theta = 0^\circ$, (b) $\theta = 2.5^\circ$, and (c) $\theta = 5^\circ$

$F_s \in [4.5, 13.6]$ N. With higher inclined angles, the areas of backward motion became larger, and the forward motion appeared in smaller ranges of the parameters. With an inclined angle of 5° , the system had forward motion in small ranges of $F_s \in [10, 13.6]$ N and $\alpha \in [0.59, 0.79]$. Generally, larger friction combined with a smaller value of the force ratio would result in faster moving forward.

4 Conclusions

This paper presented experimental results of a vibro-impact-driven locomotion system under different friction conditions, including both isotropic and anisotropic friction.

The following remarks would be useful for further studies:

- For the system working with isotropic friction, the level of preset friction force would have significant effects both on the rate and the direction of the progression.
- For the system working with anisotropic friction, the vibro-impact would provide forward motion of the whole system. Larger friction combined with a smaller value of the force ratio would result in faster moving forward.

Acknowledgments This research is funded by Vietnam National Foundation for Science and Technology Development (NAFOSTED) under grant number 107.01-2017.318.

References

1. A. Garg, C.S. Vikram, S. Gupta, M.K. Sutar, P.M. Pathak, N.K. Mehta, A.K. Sharma, V.K. Gupta, Design and development of in vivo robot for biopsy. *Mech. Based Design Struct. Mach.* **42**(3), 278–295 (2014). <https://doi.org/10.1080/15397734.2014.898587>
2. F.L. Chernous'ko, The optimum rectilinear motion of a two-mass system. *J. Appl. Math. Mech.* **66**(1), 1–7 (2002). [https://doi.org/10.1016/S0021-8928\(02\)00002-3](https://doi.org/10.1016/S0021-8928(02)00002-3)

3. Y. Yan, Y. Liu, L. Manfredi, S. Prasad, Modelling of a vibro-impact self-propelled capsule in the small intestine. *Nonlinear Dyn.* **96**(1), 123–144 (2019). <https://doi.org/10.1007/s11071-019-04779-z>
4. J. Ju, Q. Wang, K. Zhang, Design and analysis of a novel micro-robot driving platform. *Proc. Inst. Mech. Eng. C J. Mech. Eng. Sci.* **233**(11), 3849–3857 (2018). <https://doi.org/10.1177/0954406218802314>
5. T.-H. Duong, V.-D. Nguyen, H.-C. Nguyen, N.-P. Vu, N.-K. Ngo, V.-T. Nguyen, A new design for bidirectional autogenous mobile systems with two-side drifting impact oscillator. *Int. J. Mech. Sci.* **140**, 325–338 (2018). <https://doi.org/10.1016/j.ijmecsci.2018.01.003>
6. Y. Yan, Y. Liu, J. Páez Chávez, F. Zonta, A. Yusupov, Proof-of-concept prototype development of the self-propelled capsule system for pipeline inspection. *Meccanica* **53**(8), 1997–2012 (2018). <https://doi.org/10.1007/s11012-017-0801-3>
7. Z. Du, H. Fang, X. Zhan, J. Xu, Experiments on vibration-driven stick-slip locomotion: A sliding bifurcation perspective. *Mech. Syst. Signal Process.* **105**, 261–275 (2018). <https://doi.org/10.1016/j.ymsp.2017.12.001>
8. V.-D. Nguyen, H.-C. Nguyen, N.-K. Ngo, N.-T. La, A new design of horizontal electro-Vibro-impact devices. *J. Comput. Nonlinear Dyn.* **12**(6), 061002 (2017). <https://doi.org/10.1115/1.4035933>
9. Y. Liu, E. Pavlovskaia, M. Wiercigroch, Experimental verification of the vibro-impact capsule model. *Nonlinear Dyn.* **83**(1–2), 1029–1041 (2015). <https://doi.org/10.1007/s11071-015-2385-6>
10. N.A. Sobolev, K.S. Sorokin, Experimental investigation of a model of a vibration-driven robot with rotating masses. *J. Comput. Syst. Sci. Int.* **46**(5), 826–835 (2007). <https://doi.org/10.1134/s1064230707050140>
11. P. Liu, H. Yu, S. Cang, Modelling and analysis of dynamic frictional interactions of vibro-driven capsule systems with viscoelastic property. *Eur. J. Mech. A-Solids* **74**, 16–25 (2019). <https://doi.org/10.1016/j.euromechsol.2018.10.016>
12. P. Liu, H. Yu, S. Cang, On the dynamics of a vibro-driven capsule system. *Arch. Appl. Mech.* **88**(12), 2199–2219 (2018). <https://doi.org/10.1007/s00419-018-1444-0>
13. Y. Liu, E. Pavlovskaia, D. Hendry, M. Wiercigroch, Vibro-impact responses of capsule system with various friction models. *Int. J. Mech. Sci.* **72**, 39–54 (2013). <https://doi.org/10.1016/j.ijmecsci.2013.03.009>
14. A. Nunuparov, F. Becker, N. Bolotnik, I. Zeidis, K. Zimmermann, Dynamics and motion control of a capsule robot with an opposing spring. *Arch. Appl. Mech.* **89**(10), 2193–2208 (2019). <https://doi.org/10.1007/s00419-019-01571-8>
15. X. Zhan, J. Xu, H. Fang, A vibration-driven planar locomotion robot—Shell. *Robotica* **36**(9), 1402–1420 (2018). <https://doi.org/10.1017/S0263574718000383>
16. V.-D. Nguyen, T.-H. Duong, N.-H. Chu, Q.-H. Ngo, The effect of inertial mass and excitation frequency on a Duffing vibro-impact drifting system. *Int. J. Mech. Sci.* **124–125**, 9–21 (2017). <https://doi.org/10.1016/j.ijmecsci.2017.02.023>
17. J. Fan, C. Li, Z. Yang, S. Chen, J. Cao, C. Dou, On discontinuous dynamics of a 2-DOF oscillator with an one-sided rigid obstacle. *Int. J. Non-Linear Mech.* **118**, 103261 (2020). <https://doi.org/10.1016/j.ijnonlinmec.2019.103261>
18. J. Xu, H. Fang, Improving performance: recent progress on vibration-driven locomotion systems. *Nonlinear Dyn.* **98**(4), 2651–2669 (2019). <https://doi.org/10.1007/s11071-019-04982-y>
19. P. Liu, H. Yu, S. Cang, Optimized adaptive tracking control for an underactuated vibro-driven capsule system. *Nonlinear Dyn.* **94**(3), 1803–1817 (2018). <https://doi.org/10.1007/s11071-018-4458-9>
20. M.V. Golitsyna, Periodic regime of motion of a vibratory robot under a control constraint. *Mech. Solids* **53**(1), 49–59 (2018). <https://doi.org/10.3103/S002565441803007X>
21. F.L. Chernousko, Optimal control of two-dimensional motions of a body by a movable mass. *IFAC-PapersOnLine* **51**(2), 232–235 (2018). <https://doi.org/10.1016/j.ifacol.2018.03.040>

22. V.-D. Nguyen, H.-D. Ho, T.-H. Duong, N.-H. Chu, Q.-H. Ngo, Identification of the effective control parameter to enhance the progression rate of vibro-impact devices with drift. *J. Vib. Acoust.* **140**(1), 011001 (2017). <https://doi.org/10.1115/1.4037214>
23. Y. Liu, E. Pavlovskaja, M. Wiercigroch, Z. Peng, Forward and backward motion control of a vibro-impact capsule system. *Int. J. Non-Linear Mech.* **70**, 30–46 (2015). <https://doi.org/10.1016/j.ijnonlinmec.2014.10.009>
24. B. He, B.R. Wang, T.H. Yan, Y.Y. Han, A distributed parallel motion control for the multi-thruster autonomous underwater vehicle. *Mech. Based Des. Struct. Mach.* **41**(2), 236–257 (2013). <https://doi.org/10.1080/15397734.2012.726847>
25. P. Liu, M. Nazmul Huda, Z. Tang, K. Sun, A self-propelled robotic system with a visco-elastic joint: Dynamics and motion analysis. *Eng. Comput.* **36**(2), 655–669 (2019). <https://doi.org/10.1007/s00366-019-00722-3>
26. H. Yu, Y. Liu, T. Yang, Closed-loop tracking control of a pendulum-driven cart-pole underactuated system. *Proc. Inst. Mech. Eng. Part I J. Syst. Control Eng.* **222**(2), 109–125 (2008). <https://doi.org/10.1243/09596518JSCE460>
27. M.N. Huda, H. Yu, Trajectory tracking control of an underactuated capsbot. *Auton. Robot.* **39**(2), 183–198 (2015). <https://doi.org/10.1007/s10514-015-9434-3>
28. G. Su, C. Zhang, R. Tan, H.A. Li, Design of the electromagnetic driver for the internal force-static friction capsbot. In: *2009 IEEE/RSJ International Conference on Intelligent Robots and Systems*, 10–15 Oct. 2009 2009, pp 613–617. <https://doi.org/10.1109/IROS.2009.5354587>
29. H. Li, K. Furuta, F.L. Chernousko, Motion generation of the capsbot using internal force and static friction. In: *Proceedings of the 45th IEEE Conference on Decision and Control*, 13–15 Dec. 2006 2006, pp. 6575–6580. <https://doi.org/10.1109/CDC.2006.377472>
30. J. Xu, H. Fang, Stick-slip effect in a vibration-driven system with dry friction: sliding bifurcations and optimization. *J. Appl. Mech.* **81**, 061001 (2014). <https://doi.org/10.1115/1.4025747>
31. F.L. Chernous'ko, The optimal periodic motions of a two-mass system in a resistant medium. *J. Appl. Math. Mech.* **72**(2), 116–125 (2008). <https://doi.org/10.1016/j.jappmathmech.2008.04.014>
32. Y. Yan, Y. Liu, M. Liao, A comparative study of the vibro-impact capsule systems with one-sided and two-sided constraints. *Nonlinear Dyn.* **89**(2), 1063–1087 (2017). <https://doi.org/10.1007/s11071-017-3500-7>
33. E. Pavlovskaja, M. Wiercigroch, C. Grebogi, Modeling of an impact system with a drift. *Phys. Rev. E Stat. Nonlin. Soft Matter Phys.* **64**(5 Pt 2), 056224 (2001). <https://doi.org/10.1103/PhysRevE.64.056224>
34. E. Pavlovskaja, M. Wiercigroch, K.-C. Woo, A.A. Rodger, Modelling of ground Miling dynamics by an impact oscillator with a frictional slider. *Meccanica* **38**(1), 85–97 (2003). <https://doi.org/10.1023/a:1022023502199>
35. V.-D. Nguyen, K.-C. Woo, E. Pavlovskaja, Experimental study and mathematical modelling of a new of vibro-impact miling device. *Int. J. Non-Linear Mech.* **43**(6), 542–550 (2008). <https://doi.org/10.1016/j.ijnonlinmec.2007.10.003>
36. V.D. Nguyen, K.C. Woo, New electro-vibroimpact system. *Proc. Inst. Mech. Eng. C J. Mech. Eng. Sci.* **222**(4), 629–642 (2008). <https://doi.org/10.1243/09544062jmes833>
37. A.N. Grankin, S.F. Yatsun, Investigation of vibroimpact regimes of motion of a mobile microrobot with electromagnetic drive. *J. Comput. Syst. Sci. Int.* **48**(1), 155–163 (2009). <https://doi.org/10.1134/S1064230709010158>
38. K.A. Sapronov, A.A. Cherepanov, S.F. Yatsun, Investigation of motion of a mobile two-mass vibration-driven system. *J. Comput. Syst. Sci. Int.* **49**(1), 144–151 (2010). <https://doi.org/10.1134/S1064230710010156>
39. J.-H. Ho, V.-D. Nguyen, K.-C. Woo, Nonlinear dynamics of a new electro-vibro-impact system. *Nonlinear Dyn.* **63**(1–2), 35–49 (2010). <https://doi.org/10.1007/s11071-010-9783-6>
40. G. Su, C. Zhang, R. Tan, H.A. Li, Design of the electromagnetic driver for the “internal force-static friction” capsbot. In: *The 2009 IEEE/RSJ International Conference on Intelligent Robots and Systems*, 2009. IEEE, pp 613–617

41. V.-D. Nguyen, N.-T. La, An improvement of vibration-driven locomotion module for capsule robots. *Mech. Based Des. Struct. Mach.*, 1–15 (2020). <https://doi.org/10.1080/15397734.2020.1760880>
42. B. Guo, Y. Liu, R. Birler, S. Prasad, Self-propelled capsule endoscopy for small-bowel examination: proof-of-concept and model verification. *Int. J. Mech. Sci.* **174**, 105506 (2020). <https://doi.org/10.1016/j.ijmecsci.2020.105506>
43. B. Guo, E. Ley, J. Tian, J. Zhang, Y. Liu, S. Prasad, Experimental and numerical studies of intestinal frictions for propulsive force optimisation of a vibro-impact capsule system. *Nonlinear Dyn.* **101**(1), 65–83 (2020). <https://doi.org/10.1007/s11071-020-05767-4>